Asian Journal of Pharmaceutical Sciences 19 (2024) 100968

Available online at www.sciencedirect.com

ScienceDirect

journal homepage: www.elsevier.com/locate/AJPS

Cell membrane-coated mRNA nanoparticles for enhanced delivery to dendritic cells and immunotherapy

Qiaoyun Li[1], *Junho Byun*[1], *Dongyoon Kim*, *Yina Wu*, *Jaiwoo Lee*[*], *Yu-Kyoung Oh*[*]

College of Pharmacy and Research Institute of Pharmaceutical Sciences, Seoul National University, Seoul 08826, Republic of Korea

ARTICLE INFO

Article history:
Received 16 February 2024
Revised 30 June 2024
Accepted 24 July 2024
Available online 24 September 2024

Keywords:
Cell membrane coating
Dendritic cells
mRNA delivery
Immune response
Antitumor effect

ABSTRACT

Cationic polymers such as polyethylenimine have been considered promising carriers for mRNA vaccines. However, their application is hindered by their inherent toxicity and a lack of targeted delivery capability. These issues need to be addressed to develop effective cancer vaccines. In this study, we investigated whether dendritic cell membrane-coated polyethylenimine/mRNA nanoparticles (DPN) could effectively deliver mRNA to dendritic cells and induce immune responses. For comparison, we employed red blood cell membrane-coated polyethylenimine/mRNA (RPN) and plain polyethylenimine/mRNA polyplex (PN). The dendritic cell membrane coating altered the zeta potential values and surface protein patterns of PN. DPN demonstrated significantly higher uptake in dendritic cells compared to PN and RPN, and it also showed greater mRNA expression within these cells. DPN, carrying mRNA encoding luciferase, enhanced green fluorescent protein, or ovalbumin (OVA), exhibited higher protein expression in dendritic cells than the other groups. Additionally, DPN exhibited favorable mRNA escape from lysosomes post-internalization into dendritic cells. In mice, subcutaneous administration of DPN containing ovalbumin mRNA (DPN_{OVA}) elicited higher titers of anti-OVA IgG antibodies and a greater population of OVA-specific $CD8^+$ T cells than the other groups. In a B16F10-OVA tumor model, DPN_{OVA} treatment resulted in the lowest tumor growth among the treated groups. Moreover, the population of OVA-specific $CD8^+$ T cells was the highest in the DPN_{OVA}-treated group. While we demonstrated DPN's feasibility as an mRNA delivery system in a tumor model, the potential of DPN can be broadly extended for immunotherapeutic treatments of various diseases through mRNA delivery to antigen-presenting cells.

1. Introduction

Vaccines are the most effective means for humanity to prevent the spread of infectious diseases. They utilize the extraordinary capability of the highly evolved human immune system to recognize, respond to, and remember encounters with pathogen antigens. In countries with extensive vaccine program coverage, many diseases that once were major causes of childhood mortality have nearly vanished [1]. mRNA

* Corresponding authors.
E-mail addresses: ljw1112@snu.ac.kr (J. Lee), ohyk@snu.ac.kr (Y.-K. Oh).
[1] These authors contributed equally.
Peer review under responsibility of Shenyang Pharmaceutical University.

https://doi.org/10.1016/j.ajps.2024.100968

vaccines, characterized by their high potency, capacity for rapid development, and potential for low-cost production and safe administration, represent a promising strategy for treating various diseases [2]. Over the last decade, significant advancements in vaccine technologies have led to the approval of two main types of SARS-CoV-2 mRNA vaccines [3,4].

Due to its significant molecular weight (10^4–10^6 Da) and negative charge, mRNA encounters obstacles in traversing the anionic lipid bilayer of cell membranes. Furthermore, it risks being captured and degraded by nucleases through the innate immune system's cellular mechanisms. To overcome these challenges, a broad array of nanomaterials has been introduced to improve mRNA's cellular uptake and shield it from degradation [5]. Among the various mRNA delivery vehicles, lipid-based nanoparticles stand out as the most clinically advanced option, having undergone extensive research for mRNA delivery purposes. The mRNA vaccines authorized by Pfizer and Moderna, which utilize lipid nanoparticles for delivering mRNA that encodes the SARS-CoV-2 spike protein, exemplify this approach by priming the immune system [6].

Although not as clinically advanced as lipid nanoparticles, polymers offer significant benefits for mRNA delivery, demonstrating effective *in vitro* and *in vivo* mRNA delivery [7]. Polymeric mRNA delivery vehicles have captured significant interest due to their feasible synthetic versatility, structural diversity, and enhanced stability [7]. A recent study reported an inhalable polymer-based vehicle designed for therapeutic mRNA delivery, showing expression in the lung and inducing a robust immune response [8]. In another study, bioreducible polymer nanocarriers have been engineered for mRNA delivery to the spleens, leading to effective antitumor therapy in mice [9].

Despite the advantages of cationic polymers for mRNA delivery, they suffer from a lack of targeting capability. Polyethylenimine (PEI), one of the most widely studied cationic polymers, can form polyplexes with mRNA through electrostatic interaction, and has been studied to enhance the cellular uptake and endosomal escape of mRNA. Due to the simple mixing step, PEI polyplexes have advantages in cost efficiency and manufacturing processes. However, the lack of targeting capacity of PEI polyplexes has limited their applications in the treatment of immune cell-related diseases. Approaches have been made to provide targeting capability through covalent structural modifications with ligand molecules [10].

Meanwhile, cell membrane coating of nanoparticles has emerged as a new class of biomaterials, offering multifunctional capabilities to the nanocores. These nanocores act as matrices for encapsulating therapeutic agents, while the cell membrane coating facilitates effective interactions with proteins, and cells within the body [11]. As sources of membranes, red blood cells [12], cancer cells [13], leukocytes [14], and vaginal endothelial cells [15,16] have been studied. Red blood cell membranes have been studied to achieve extended *in vivo* retention times [12]. Cancer cell membranes have been studied to coat the surfaces of nanoparticles and increase the delivery of nanoparticles to tumor cells [13]. Leukocyte membranes have been employed for their effectiveness in navigating vascular barriers by reducing opsonization, utilizing self-recognition mechanisms to delay phagocytic uptake, binding to inflamed endothelium, and facilitating transport across the endothelial layer while avoiding the lysosomal pathway [14]. Vaginal endothelial cell membranes have been studied for shielding cells against toxins [15]. Additionally, membranes from neutrophils [17], mesenchymal stem cells [18], fibroblasts [19], and embryonic kidney cells [20] have been enlisted for specific targeting purposes.

Although various cells have been studied as sources of membranes to coat the surfaces of nanoparticles, dendritic cells have not been widely studied as sources of membrane for coating nanocores. Dendritic cells, as specialized antigen-presenting cells, are pivotal in initiating and regulating both innate and adaptive immune responses. Notably, dendritic cell-derived vesicles, including exosomes, have demonstrated the capability in targeting specific immune cells such as antigen-presenting cells and T cells [21]. Several studies have reported that vesicles from dendritic cells showed increased internalization into dendritic cells due to a homing effect and surface molecules [22,23]. In particular, major histocompatibility complex (MHC) molecules and CD11a, which are involved in interactions between dendritic cells, play a crucial role in the targeting mechanism [24,25]. However, few studies have been done to use dendritic cells for membrane coating of cationic mRNA nanocores.

In this study, we proposed that coating mRNA nanocores with dendritic cell membranes could enhance their delivery to dendritic cells and subsequent immune responses. To test the hypothesis, we constructed a polyethylenimine/mRNA nanocore (PN) and coated this core with dendritic cell membranes to form a dendritic cell membrane-coated polyethylenimine/mRNA nanocarrier (DPN) (Fig. 1A). Utilizing OVA mRNA as a model antigen, we examined the efficacy of DPN in delivering mRNA to dendritic cells and eliciting immune responses (Fig. 1B).

2. Materials and methods

2.1. *Materials*

Mouse bone marrow-derived dendritic cells (BMDC) were isolated and cultured as previously described [26]. In brief, bone marrow was harvested from the femurs and subjected to erythrocyte lysis. For BMDC differentiation, the cells were incubated in complete Iscove's Modified Dulbecco's Medium (IMDM) supplied by Welgene (Gyeongsangbuk-do, Republic of Korea), enriched with 100 units/ml of penicillin, 100 μg/ml of streptomycin (Capricorn Scientific GmbH, Hesse, Germany), 10 % heat-inactivated bovine serum (Gibco, New York, NY, USA), 20 ng/ml of recombinant mouse granulocyte-macrophage colony-stimulating factor (GM-CSF, GenScript, Piscataway, NJ, USA), interleukin-4 (IL-4, GenScript), and 50 μM β-mercaptoethanol (Sigma-Aldrich, Burlington, MA, USA). The differentiation process spanned 7 d before the cells were ready for experimental use.

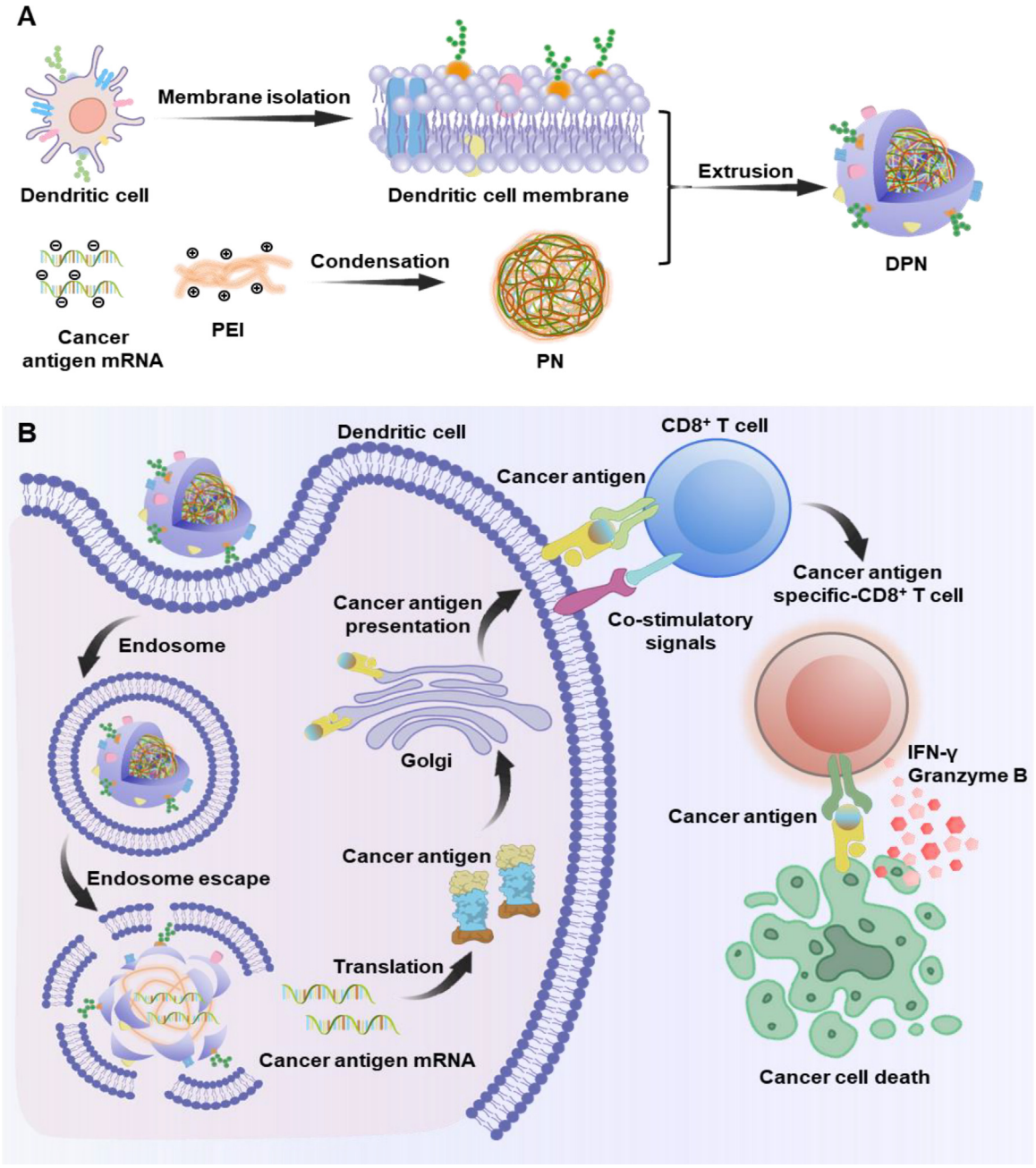

Fig. 1 – DPN-mediated delivery of mRNA and induction of antigen-specific immune responses. (A) The construction of DPN is illustrated. mRNA was complexed with PEI, forming PN. Subsequently, PN was coated with dendritic cell membrane materials through co-extrusion processes, resulting in DPN. (B) Proposed mechanism of DPN is depicted. After DPN was internalized by dendritic cells, mRNA escaped from endosome to the cytoplasm. Antigen protein translated from mRNA was presented on the dendritic cell surfaces by the major histocompatibility complex molecules. The antigen-presenting dendritic cells primed T cells, establishing an antigen-specific immune response. Cancer cells could be killed when these antigen-specific CD8$^+$ T cells recognized corresponding antigens in the cancer cell membrane.

Ovalbumin-expressing B16F10 melanoma cell line (B16F10-OVA, kindly provided by Prof. Youngro Byun (Seoul National University, Seoul, Republic of Korea) was maintained in complete Dulbecco's modified Eagle's medium (DMEM, Welgene) supplemented with 100 units/ml of penicillin, 100 μg/ml of streptomycin (Capricorn Scientific GmbH), and 10 % heat-inactivated bovine serum (Gibco, New York, NY, USA).

2.2. *Isolation of cell membranes*

Dendritic cell membrane materials were prepared according to previously reported method with slight modifications [13]. Cells were lysed in a hypotonic buffer (20 mM Tris–HCl pH 7.5, 10 mM KCl, 2 mM $MgCl_2$, protease inhibitor) using a Dounce homogenizer. The lysate was centrifuged at 20,000 × *g* for 20 min to remove cell debris, and the clear supernatant was

further centrifuged at 100,000 × *g* for 1 h to collect the plasma membrane material. This pellet was washed with 10 mM HEPES (pH 7.5) and used as purified membrane material. In certain experiments, for comparison purposes with dendritic cell membranes, red blood cell materials were prepared using a hypotonic lysis method [27]. The total protein content of the purified membranes was quantified using the bicinchoninic acid (BCA) assay, and the membrane concentration was adjusted to 1 mg/ml for subsequent studies.

2.3. Characterization of cell membrane

The protein pattern of the isolated cell membrane was analyzed using sodium dodecyl sulfate-polyacrylamide gel electrophoresis (SDS-PAGE). Samples were first dissolved in pre-cold radioimmunoprecipitation assay buffer (RIPA lysis buffer, ROCKLAND, Royersford, PA, USA) on ice for 30 min. Separation of proteins was performed using a 10 % polyacrylamide gel (SMOBiO Technology, Hsinchu, Taiwan, ROC) and the Novex Xcell Surelock Electrophoresis System (Bio-Rad, Hercules, CA, USA). Subsequently, the protein gel was stained overnight at 4 °C with Coomassie Brilliant Blue protein staining buffer (Bio-Rad) and destained with triple distilled water (TDW) for 6 h before photography.

2.4. Construction of polyplex and nanoparticles

Nanoparticles were prepared by forming a polyplex mRNA core and cloaking it with cell membrane materials. Polyplex mRNA core was prepared using linear polyethylenimine (MW 25,000, Polysciences, Warrington, PA, USA). A stock solution of PEI was prepared at 1 mg/ml and stored at −20 °C. PEI and OVA mRNA (TriLink Biotechnologies, San Diego, CA, USA) were separately diluted in 25 mM sodium acetate buffer (pH 5.0) before being combined at a 3:1 (w/w) ratio, a condition maintained throughout the study unless noted otherwise. This mixture was allowed to self-assemble into a polyplex PEI/mRNA nanocore (PN) for 5 min, achieving an mRNA concentration of 50 μg/ml. In certain experiments, PEI was complexed with cyanine 5 (Cy5)-conjugated enhanced green fluorescent protein (EGFP) mRNA (ApexBio Technology, Houston, TX, USA), resulting in PEI/Cy5-conjugated EGFP mRNA nanocores (Cy5PN).

The polyplex mRNA core was coated with cell membrane materials using a previously reported extrusion method, with minor modifications [28]. Dendritic cell membrane materials were mixed with PN or Cy5PN at a 1:4 (v/v) ratio. This mixture was then extruded sequentially through 400 and 200 nm polycarbonate membranes (Merck Millipore, Burlington, MA, USA), resulting in the formation of dendritic cell membrane-coated PEI/OVA mRNA nanoparticles (DPN) or dendritic cell membrane-coated Cy5PN (DCy5PN). In some experiments, red blood cell membrane materials were utilized to coat PN or Cy5PN, yielding red blood cell membrane-coated PN (RPN) or red blood cell membrane-coated Cy5PN (RCy5PN).

To evaluate the membrane coating of the polyplex mRNA core, Cy5PN was coated with the cell membrane labeled with 3,3′-dioctadecyloxacarbocyanine perchlorate (DiO, Invitrogen, Carlsbad, CA, USA). The population of $DiO^{+}Cy5^{+}$ particles was analyzed with a BD FACS Lyric flow cytometry system (BD Biosciences, San Jose, CA, USA).

2.5. Gel retardation and RNA assays

The gel retardation assay was conducted to assess the formation of polyplexes between PEI and OVA mRNA (TriLink Biotechnologies). These components were mixed at varying w/w ratios (0.12:1, 0.6:1, 3:1, 15:1) and incubated for 5 min to allow for self-assembly. The resultant polyplexes were then analyzed using electrophoresis on a 1 % agarose gel. To evaluate the efficiency of OVA mRNA complexation with linear PEI, the RiboGreen RNA assay (Invitrogen) was employed according to the manufacturer's instructions [29]. For this assay, polyplexes at different weight ratios were dispensed into a 96-well black plate. Following the addition of the RiboGreen reagent, fluorescence intensities were measured using a SpectraMax® M5 multi-reader (Molecular Devices, Silicon Valley, CA, USA). The complexation efficiency was determined by comparing the amount of mRNA complexed to the total amount of mRNA added.

2.6. Characterization of nanoparticles

Characterization of various nanoparticles was conducted in terms of size distribution, zeta potential, transmission electron microscopy (TEM), and stochastic optical reconstruction microscopy (STORM). The size distribution and zeta potential of PN, RPN and DPN were determined using the dynamic light scattering method and laser Doppler microelectrophoresis at a 22° angle with an ELS8000 instrument (Photal, Osaka, Japan).

TEM images were acquired using a transmission electron microscope (JEM-2100PLUS, JEOL, Tokyo, Japan) to observe the membrane coating of the mRNA core. Nanoparticles were placed on a grid and allowed to adhere for analysis. To visualize the dendritic cell membrane coating, major histocompatibility complex class II (MHC class II) molecules on dendritic cell membranes were stained with a rat anti-mouse I-A/I-E antibody (1:100, Biolegend, San Diego, CA, USA), followed by incubation with a 10 nm gold-conjugated anti-rat IgG antibody (1:100, Abcam, Cambridge, UK) at room temperature for 1 h.

For STORM imaging, Cy5PN were coated with a DiO-labeled cell membrane. These nanoparticles were then placed on poly-l-lysine coverslips (Corning, New York, NY, USA). The samples were immersed in STORM buffer, which consists of glucose oxidase (0.8 mg/ml, Sigma-Aldrich), catalase (40 μg/ml, Sigma-Aldrich), glucose (5 %, w/v), and cysteamine (100 mM, Sigma-Aldrich) in a 50 mM Tris–HCl buffer (pH 8.0) [30]. STORM imaging was performed on a Nikon STORM system (TiA1-N-STORM, Nikon, Tokyo, Japan), set up for total internal reflection fluorescence (TIRF) imaging. Images were captured over a 256 × 256-pixel area (pixel size 0.16 μm) with a 20-ms integration time.

2.7. Cellular uptake study

The uptake of nanoparticles by dendritic cells was assessed via flow cytometry. Dendritic cells were exposed to Cy5PN

coated with cell membranes, at an mRNA concentration of 0.5 μg/ml. After varying treatment durations, dendritic cells were stained with fluorescein isothiocyanate (FITC)-conjugated anti-mouse CD11c antibody (1:100, Biolegend). Cellular fluorescence was analyzed using a BD FACS Lyric flow cytometry system (BD Biosciences).

To compare the cellular uptake of nanoparticles in different immune cells, the uptake of nanoparticles was assessed using splenocytes. Briefly, splenocytes were treated with various nanoparticles containing Cy5-tagged mRNA at an mRNA concentration of 0.5 μg/ml for 2 h. Splenocytes were stained with PerCP/Cy5.5-tagged anti-mouse I-A/I-E antibody (1:100, Biolegend), FITC-tagged anti-mouse CD11c antibody (1:100, Biolegend), phycoerythrin (PE)-tagged anti-mouse CD19 antibody (1:100, Biolegend), Alexa Fluor 700-tagged anti-mouse F4/80 antibody (1:100, Biolegend), PE-tagged anti-mouse CD11b antibody (1:100, Biolegend), and FITC-tagged anti-mouse Ly6G antibody (1:100, Biolegend). Cellular uptake of nanoparticles was determined using a BD FACS Lyric flow cytometry system (BD Biosciences).

2.8. *Intracellular trafficking of nanoparticles*

Intracellular trafficking of nanoparticles was examined using immunofluorescence staining, following previous methods with minor adjustments [31]. Dendritic cells were treated with various nanoparticles at a concentration of 0.5 μg/ml mRNA for 2 h followed by additional incubation for 0.5, 1 and 4 h. To study the effect of PEI on endo/lysosome escape, dendritic cells were pretreated with bafilomycin A1 for 1 h at 200 nM, followed by nanoparticle treatment [32,33]. The endo/lysosomes of dendritic cells were stained with LysoTracker™ Red DND-99 (Invitrogen) according to the manufacturer's protocol. Briefly, cells were incubated with 50 nM LysoTracker solution for 30 min and fixed with 4 % paraformaldehyde. After fixation, nuclei were stained with 1 μM 4′,6-diamidino-2-phenylindole (DAPI, Sigma-Aldrich). Cellular fluorescence was observed using a TCS SP8 Confocal Microscope (Leica, Wetzlar, Germany). Pearson's correlation coefficient at different time points was calculated using Image J (National Institutes of Health, Bethesda, MD, USA).

2.9. *Cellular expression of mRNA delivered by nanoparticles*

To assess mRNA delivery by nanoparticles, three mRNA types, luciferase mRNA (Luc mRNA, TriLink Biotechnologies), EGFP mRNA, and OVA mRNA, were encapsulated. The *in vitro* antigen expression of the mRNA vaccine was evaluated using a previously reported method, with slight modifications [34,35]. Dendritic cells were treated with nanoparticles containing 0.5 μg/ml mRNA for 2 h and then medium was replaced. After 24 h, exogenous mRNA expression was evaluated using luciferase assay, flow cytometry, or microscopy.

The luciferase mRNA expression was assessed using the Luciferase Assay System kit (Promega™ Corporation, Madison, WI, USA) following the manufacturer's instructions. Luminescence was measured with a luminometer (Centro LB 960, Berthold, Bad Wildbad, Baden-Wurttemberg, Germany) and imaged using a biomolecular imaging system (ImageQuant 800 F, Cytiva, Marlborough, MA, USA).

To assess EGFP mRNA expression, dendritic cells were stained with PE-conjugated anti-mouse CD11c antibody (1:100, Biolegend). EGFP mRNA expression was visualized using a TCS SP8 Confocal Microscope (Leica) and further examined by flow cytometry (BD FACS Lyric flow cytometry system, BD Biosciences), with dendritic cells stained with PE-conjugated anti-mouse CD11c antibody (1:100, Biolegend).

For OVA mRNA transfection, dendritic cells were stained with FITC-conjugated anti-mouse CD11c antibody (1:100, Biolegend) and allophycocyanin (APC)-conjugated anti-mouse H-2K^b bound to SIINFEKL antibody (1:100, Biolegend) for 1 h. Importantly, all procedures involving the H-2K^b bound to SIINFEKL antibody were conducted without fixation and permeabilization to ensure the detection of OVA localized on the dendritic cell membrane. Fluorescence intensity was analyzed using flow cytometry (BD Biosciences), and surface OVA presentation was observed using a confocal microscope (Leica).

2.10. *Animal*

Five-week-old C57BL/6 mice were supplied from Raon Bio (Raon Bio Korea, Yongin, Republic of Korea) and housed in standard pathogen-free conditions at the Animal Center for Pharmaceutical Research, Seoul National University. All experiments were conducted in accordance with the Guidelines for the Care and Use of Laboratory Animals of the Institute of Laboratory Animal Resources, Seoul National University (Approval number: SNU-210106-4).

2.11. *Enzyme-linked immunosorbent spot assay*

To study antigen-specific immune responses, mice received subcutaneous injections of various nanoparticles three times per week, each containing 10 μg OVA mRNA. One week after the third injection, splenocytes were harvested. Splenocytes were obtained by passing spleens through 70 μm cell strainers and lysing red blood cells with ACK lysis buffer (Gibco). Subsequently, 2×10^6 splenocytes per well were stimulated for 24 h with 5 μg/ml $OVA_{257–264}$ peptide (SIINFEKL, GenScript). The number of spots produced by interferon-γ (IFN-γ) - secreting cells was determined using an enzyme-linked immunosorbent spot (ELISpot) kit (BD Biosciences) following the manufacturer's instructions.

2.12. *Measurement for anti-OVA antibody titer*

C57BL/6 mice received subcutaneous injections of various nanoparticles three times, each containing 10 μg of OVA mRNA. One week after the third injection, blood was collected to quantify OVA-specific IgG levels in the plasma using enzyme-linked immunosorbent assay (ELISA). Anti-mouse IgG antibody conjugated with horseradish peroxidase (HRP, Santa Cruz Biotechnology, Santa Cruz, Dallas, TX, USA) was utilized to detect anti-OVA IgG antibody. Optical densities were measured at 450 nm using an absorbance microplate reader (Sunrise™, Tecan, Männedorf, canton of Zürich,

Switzerland) after the addition of horseradish peroxidase substrates.

2.13. Determination of OVA-specific $CD8^+$ T cells

One week after three subcutaneous administrations of OVA mRNA-containing nanoparticles, spleens were harvested to assess OVA-specific $CD8^+$ T cells. Splenocytes were restimulated with 10 μg/ml of $OVA_{257–264}$ peptide (SIINFEKL, GenScript) for 72 h. The splenocytes were then incubated with PE-conjugated MHC tetramer specific for $CD8^+$ T cells recognizing OVA epitope SIINFEKL (1:100, MBL International Corporation, Woburn, MA, USA) for 30 min. Subsequently, the cells were stained with FITC-conjugated anti-mouse CD3 antibody (1:100, Biolegend) and PerCP/Cy5.5-conjugated anti-mouse CD8 antibody (1:100, Biolegend) for 1 h. Data were acquired using a BD LSRFortessa™ X-20 Flow Cytometer (BD Biosciences) with the BD FACS Diva software (BD Biosciences) and analyzed using the FlowJo software (FlowJo, Ashland, OR, USA).

2.14. Immune activation via subcutaneous administration of DPN_{OVA}

To evaluate the effect of DPN_{OVA} on immune activation, five-week-old C57BL/6 mice were subcutaneously injected with 1×10^5 B16F10-OVA cells into the right flank. On Day 4 post-tumor cell inoculation, mice were randomly assigned to different groups and received four subcutaneous administrations of DPN_{OVA}, at a dose of 10 μg OVA mRNA. One day after the last injection, lymph nodes were harvested for further analysis. To obtain single cells, lymph nodes were passed through 70 μm cell strainers. To investigate DC maturation in lymph nodes, cells were stained with APC-tagged anti-mouse CD40 antibody (1:100, Biolegend), APC-tagged anti-mouse CD86 antibody (1:100, Biolegend), and FITC-tagged anti-mouse CD11c antibody (1:100, Biolegend) for 1 h at room temperature. Data were acquired using a BD FACS Lyric flow cytometry system (BD Biosciences).

To determine T cell activation, spleens were harvested after subcutaneous administration of DPN_{OVA} and splenocytes were prepared for further analysis. Splenocytes were treated with DPN_{OVA} at a dose of 0.5 μg/ml OVA mRNA for 2 h. After an additional 48-hour incubation, splenocytes were stimulated with phorbol 12-myristate-13-acetate (50 ng/ml), ionomycin (1 μM) and brefeldin A (5 μg/ml) for 4 h. Subsequently, cells were stained with PerCP/Cy5.5-tagged anti-mouse CD8 antibody (1:100, Biolegend). Intracellular staining for IFN-γ and Granzyme B (GzmB) was conducted using the True Nuclear Transcription Factor Buffer Set (BioLegend). After fixation, intracellular staining was performed with PE-tagged anti-mouse IFN-γ antibody (1:100, Biolegend) and Alexa Fluor 647-tagged anti-mouse Granzyme B antibody (1:100, Biolegend). The data were acquired using a BD FACS Lyric flow cytometry system (BD Biosciences).

2.15. In vivo study of anti-tumor efficacy

In primary B16F10-OVA tumor models, the *in vivo* anti-tumor efficacy was evaluated. Five-week-old C57BL/6 mice were subcutaneously injected with 1×10^5 B16F10-OVA cells into the right flank. On Day 4 post-tumor cell inoculation, mice were randomly assigned to different groups and received 4 times of subcutaneous administration of various mRNA formulations, at a dose of 10 μg OVA mRNA. The drug administration intervals were set to twice a week over two weeks, as previously reported for uses of therapeutic cancer vaccines with slight modifications [36,37]. Tumor measurements were taken using calipers, and tumor volumes were calculated using the formula $a \times b^2 \times 0.5$, where 'a' represents the largest dimension and 'b' represents the smallest dimension. After 3 weeks, mice were euthanized for further experiments. Immune cells in tumor tissues were profiled using a BD LSRFortessa™ X-20 Flow Cytometer (BD Biosciences) with the BD FACS Diva software (BD Biosciences) and analyzed using the FlowJo software (FlowJo).

To investigate the suppressive effect of DPN_{OVA} on lung metastasis, five-week-old C57BL/6 mice were subcutaneously injected with 1×10^5 B16F10-OVA cells into the right flank. On Day 4 post-tumor cell inoculation, mice were randomly assigned to different groups and received four subcutaneous administrations of DPN_{OVA} at a dose of 10 μg OVA mRNA. On Day 14 post-tumor cell inoculation, 2×10^5 B16F10-OVA cells were intravenously injected. Mice were sacrificed and lungs were harvested for further analysis on Day 28 after inoculation.

2.16. Immunohistochemistry

OVA presentation in lymph nodes was assessed through immunohistochemistry. Two days post subcutaneous injection with each formulation (10 μg OVA mRNA per mouse), lymph nodes were collected. Paraffin-embedded sections were deparaffinized in xylene and rehydrated in ethanol. Target Retrieval Solution (pH 6.0, Agilent Dako, Santa Clara, CA, USA) was applied at 121 °C for 1 min, followed by cooling at room temperature for 30 min. Tissue sections were permeabilized with 0.1 % Triton-X100, then stained overnight at 4 °C with FITC-conjugated anti-mouse CD11c antibody (1:100, Biolegend) and APC-conjugated anti-mouse $H\text{-}2K^b$ bound to SIINFEKL antibody (1:100, Biolegend). After washing, nuclei were labeled with 1 μM DAPI (Sigma-Aldrich). Fluorescence images were captured using a THUNDER imaging system (Leica).

2.17. Safety assessment

To evaluate the safety of DPN_{OVA}, five-week-old C57BL/6 mice were subcutaneously injected with DPN_{OVA} on Day 0, 4, 7 and 11 at a dose of 10 μg OVA mRNA. Plasma was collected on Day 12 for further analysis. The levels of alanine transaminase (ALT), aspartate transaminase (AST), alkaline phosphatase (ALP), blood urea nitrogen (BUN), creatinine, and albumin were determined to evaluate liver and kidney injury.

2.18. Statistical analysis

One-way analysis of variance (ANOVA) with Tukey's post-hoc test evaluated experimental data statistically. Student's *t*-test

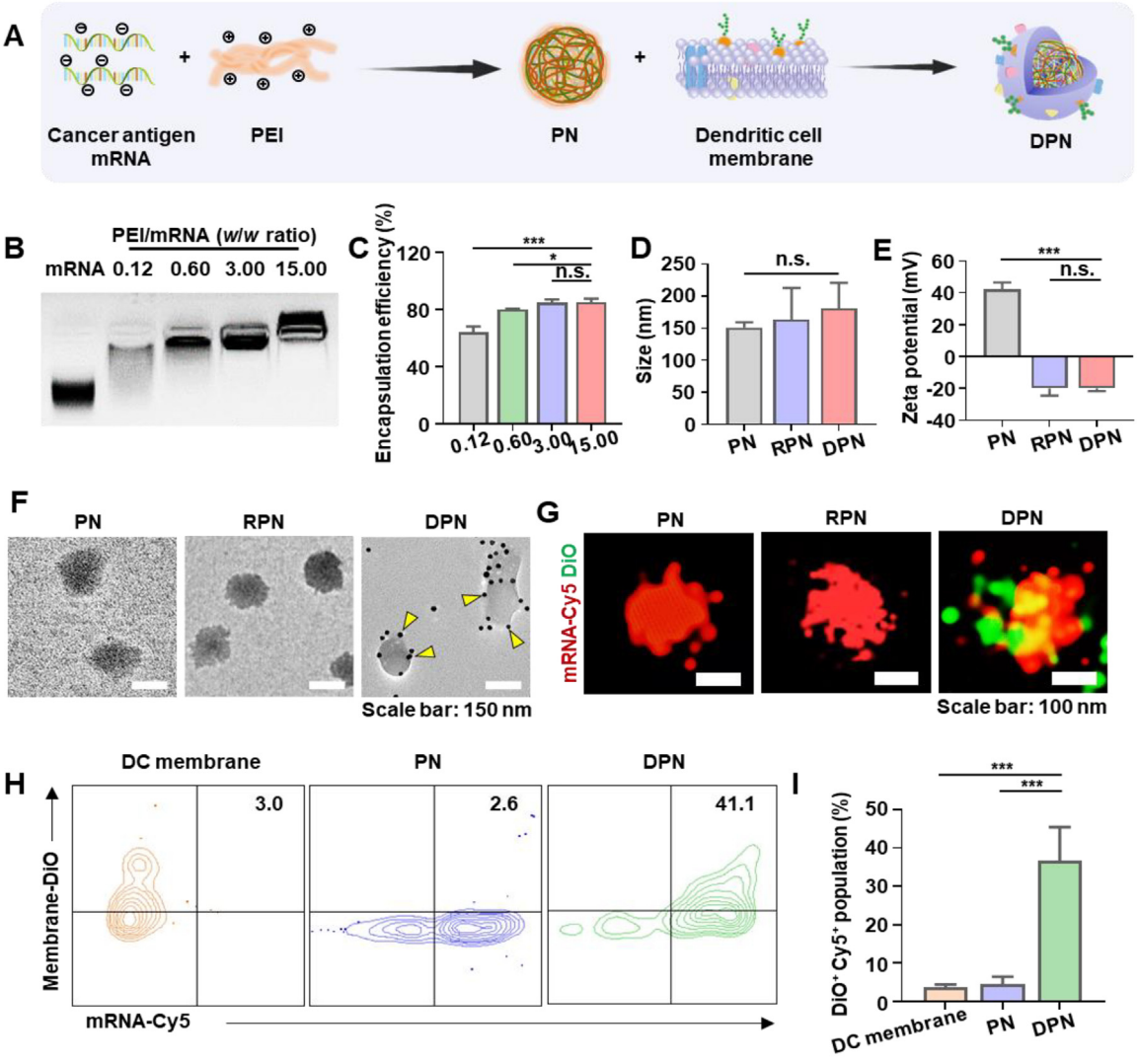

Fig. 2 – Characteristics of nanoparticles. (A) DPN fabrication involved PEI complexing with mRNA, followed by dendritic cell membrane coating on the resulting PN. (B) Electrophoresis on 1% agarose gel was used for sample analysis. (C) The efficiency of mRNA-PEI complexation was quantified by comparing complexed mRNA to total mRNA ($n = 5$). (D) Nanoparticle sizes were determined via dynamic light scattering ($n = 5$). (E) Zeta potential measurements were compared for PN, RPN, and DPN ($n = 5$). (F) TEM images of nanoparticles. Yellow arrows indicate 10 nm gold-labeled MHC class II molecules in dendritic cell membranes. (G) STORM imaging visualized nanoparticles comprising Cy5-labeled mRNA (red) and DiO-labeled dendritic cell membrane (green). (H) Flow cytometry showed the fluorophore labeled-dendritic cell membranes and Cy5-mRNA in nanoparticles, identifying DiO^+Cy5^+ DPN populations. (I) Flow cytometry quantified the DiO^+Cy5^+ populations ($n = 5$). (n.s., not significant; *$P < 0.05$; ***$P < 0.001$).

compared two groups. Statistical analyses were conducted using GraphPad Prism software (version 8.0, GraphPad Software, San Diego, CA, USA). A *P*-value <0.05 indicated statistical significance.

3. Results and discussion

3.1. *Characterization of nanoparticles*

DPN was constructed by enveloping PN with a dendritic cell membrane, as shown in Fig. 2A. In the gel retardation assay, indistinct bands were observed between the loading wells and the naked mRNA band at low PEI/mRNA ratios (0.12 and 0.6 of PEI) (Fig. 2B). At these low ratios, only some mRNA molecules could interact with PEI, resulting in PEI/mRNA complexes of heterogeneous sizes and structures. This variability in complex formation led to multiple mobility bands of mRNA, a phenomenon also observed in another study [38]. With increasing amounts of PEI, all mRNA molecules were complexed with PEI, resulting in the loss of their mobility and retention in the loading wells at a PEI to mRNA ratio of 3 or higher. Similar mRNA complexation efficiency was observed at 3:1 and 15:1 (w/w) ratios (Fig. 2C).

Herein, dendritic cell membrane materials were utilized to direct the tropism of membrane-coated nanoparticles towards dendritic cells. Several coating methods have been reported previously, including sonication, mechanical extrusion, and microfluidics. In this study, we fabricated DPN using the extrusion method, which is the most well-established method [39,40]. Membrane coating did not significantly affect nanoparticle sizes (Fig. 2D), although it altered zeta potential values, decreasing from 42.2 ± 4.3 mV for PN to −20.1 ± 4.4 mV for RPN and −20.1 ± 1.6 mV for DPN, respectively (Fig. 2E). TEM imaging revealed the spherical morphology of PN, RPN, and DPN, with DPN uniquely displaying MHC class II molecules due to the dendritic cell membrane coating (Fig. 2F). STORM imaging indicated dendritic cell membrane coating in DPN (Fig. 2G). Flow cytometry analysis showed the presence of a $DiO^{+}Cy5^{+}$ population in DPN, specifically 36.6 % ± 8.9 % (Fig. 2H and 2I). Comparative SDS-PAGE analysis revealed distinct membrane protein profiles between DPN and RPN (Fig. S1).

Although we encapsulated mRNA in DPN, the strategy of dendritic cell membrane coating has potential for delivering various cargoes, including chemical drugs and other biological substances. The delivery of tumor antigen to dendritic cells was achieved using a photosensitizer coated with a hybrid membrane derived from dendritic cells and tumor cells, following photodynamic therapy [39]. A recent study reported the delivery of rapamycin-loaded nanoparticles coated with dendritic cell membrane to immature dendritic cells, stimulating their maturation [41].

3.2. *Dendritic cell uptake of mRNA delivered by nanoparticles*

Cell membrane type influenced the uptake of membrane-coated nanoparticles by dendritic cells. DPN showed significantly enhanced uptake by dendritic cells compared to PN and RPN. Flow cytometry data showed that at 30 min post-treatment, DPN-treated groups exhibited a 2.6-fold and 1.3-fold increase in cellular uptake relative to the PN and RPN groups, respectively (Fig. 3A and 3B). This trend persisted at 1 h post-treatment, with DPN internalization significantly exceeding that of PN and RPN (Fig. 3C and 3D). Consistent with flow cytometry findings, confocal imaging revealed a higher uptake of DPN by dendritic cells in comparison to PN and RPN (Fig. 3E). Cell membrane coating can facilitate higher uptake by the same type of cells. Our findings are consistent with recent studies that have reported cell membrane coatings can exhibit tropism towards their progenitor cells [13]. Tumor cell membrane-coated nanoparticles have been reported to show tropism to tumor tissues [11].

Furthermore, DPN exhibited greater capability to escape from endo/lysosome (Fig. 3F). Pearson's correlation coefficient decreased by 3.3-fold at 4 h compared to 1 h after DPN treatment (Fig. 3G). In contrast to dendritic cells, DPN exhibited similar cellular uptake in other immune cells as PN and RPN (Fig. S2). Bafilomycin A1, a proton pump inhibitor, is known to inhibit endosome escape mediated by the proton sponge effect [32,33]. It was observed that mRNA delivered by DPN could escape from endo/lysosomes, a process inhibited by bafilomycin A1 treatment (Fig. S3). Therefore, the endo/lysosome escape observed with DPN may be partially attributed to the proton sponge effect of PEI, as previously reported [42,43]. Previous studies have demonstrated that the delivery of plasmid DNA or mRNA using PEI facilitates the escape of nucleic acids to the cytoplasm through the proton sponge effect.

3.3. *Expression of mRNA delivered by nanoparticles*

The impact of dendritic cell membrane coating on mRNA expression within dendritic cells was investigated using mRNAs encoding luciferase, EGFP, or OVA. The delivery and expression of these exogenous mRNAs by nanoparticles were assessed through luminescence for luciferase mRNA, fluorescence for EGFP mRNA, and MHC class I-mediated OVA antigen presentation for OVA mRNA in dendritic cells. Dendritic cells treated with luciferase mRNA-encapsulated DPN (DPN_{Luc}, Fig. 4A) exhibited significantly enhanced luminescence compared to the groups treated with PEI/luciferase mRNA polyplex (PN_{Luc}), and RPN carrying luciferase mRNA (RPN_{Luc}) (Fig. 4B), with luminescence intensity in the DPN_{Luc}-treated group being 3.9-fold and 1.7-fold higher than that in the PN_{Luc} and RPN_{Luc}-treated groups, respectively (Fig. 4C).

When dendritic cells were treated with EGFP mRNA-encapsulated DPN (DPN_{EGFP}, Fig. 4D), EGFP expression fluorescence was markedly higher in the DPN_{EGFP} group than in those treated with PEI/EGFP mRNA polyplex (PN_{EGFP}) and RPN carrying EGFP mRNA (RPN_{EGFP}) (Fig. 4E). The DPN_{EGFP}-treated group saw a 2.2-fold and 1.8-fold increase in $EGFP^{+}$ dendritic cells compared to the PN_{EGFP} and RPN_{EGFP}-treated groups, respectively (Fig. 4F and 4G). Exploring mRNA vaccine potential, dendritic cells treated with OVA mRNA-encapsulated DPN (DPN_{OVA}, Fig. 4H) exhibited OVA antigen presentation on their surfaces, as confirmed by confocal microscopy. This antigen presentation was notably absent in cells treated with PEI/OVA mRNA polyplex (PN_{OVA}) and RPN carrying OVA mRNA (RPN_{OVA}), but evident in the DPN_{OVA} group (Fig. 4I). Flow cytometry showed OVA presentation in the DPN_{OVA}-treated group was 2.6-fold and 2.4-fold higher than that in the PN_{OVA} and RPN_{OVA}-treated groups, respectively (Fig. 4J and K). Although both PN and DPN can leverage the proton sponge effect of PEI, the enhanced protein expression observed with DPN highlights the critical role of increased mRNA entry into the target cells.

3.4. *In vivo immune responses by DPN_{OVA}*

To evaluate DPN's effectiveness as an mRNA vaccine delivery system, the immune responses elicited by DPN_{OVA} were examined. OVA mRNA served as the model antigen and was incorporated into PN_{OVA}, RPN_{OVA}, and DPN_{OVA} formulations. In C57BL/6 mice, these OVA mRNA-containing nanoparticles were administered subcutaneously, and subsequent immune responses were assessed (Fig. 5A).

The ELISpot assay revealed that the DPN_{OVA}-treated group had significantly larger populations of cells secreting IFN-γ upon re-stimulation with $OVA_{257–264}$ peptide (Fig. 5B). IFN-γ spot counts in the DPN_{OVA} group were 1.9-fold and 1.8-fold higher than those in the PN_{OVA} and RPN_{OVA} groups,

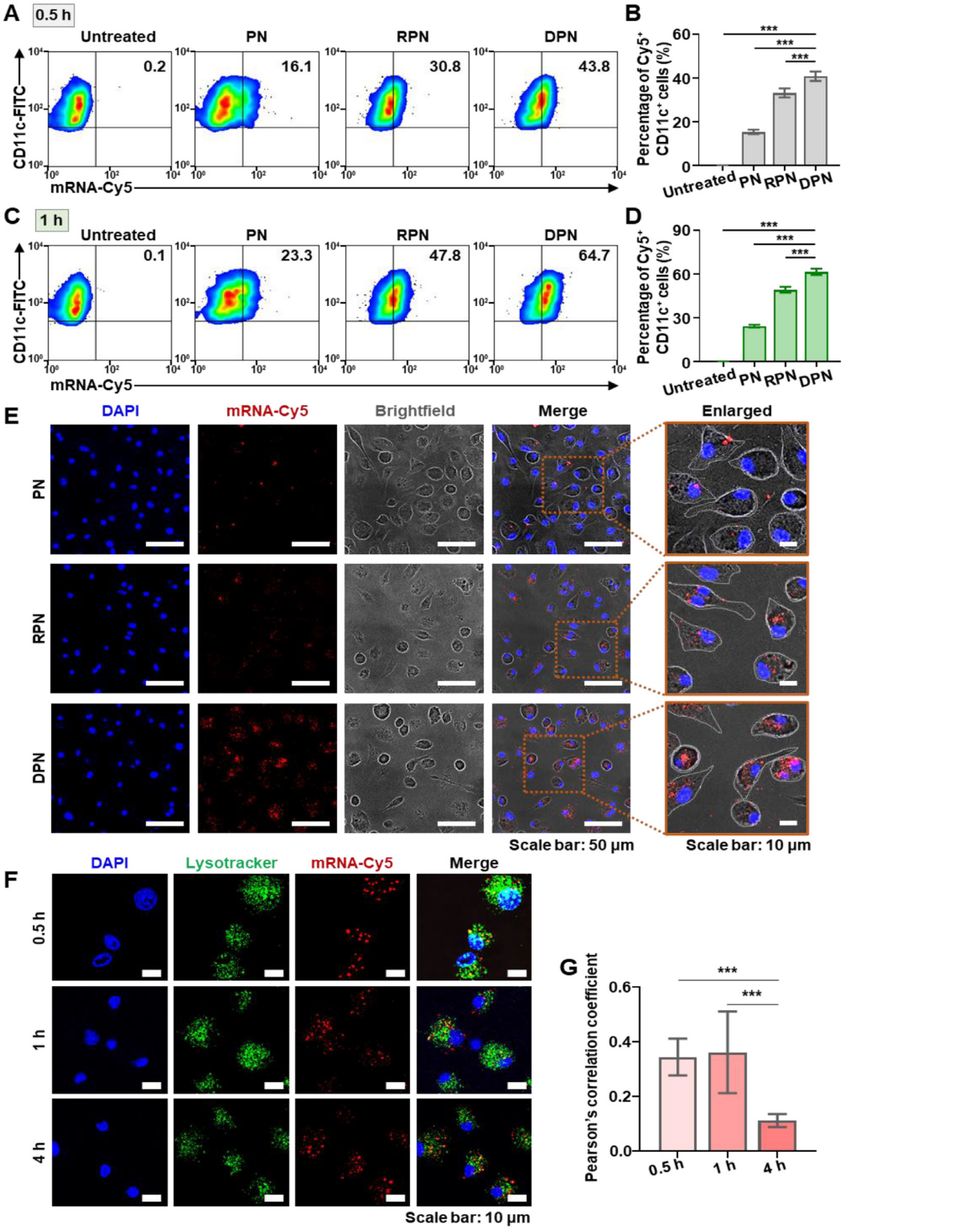

Fig. 3 – Cellular uptake of nanoparticles and mRNA trafficking. (A-D) Dendritic cells, either untreated or treated with Cy5-labeled EGFP mRNA nanoparticles, were assessed for $CD11c^+Cy5^+$ populations at 30 min (A-B) and 1 h (C-D) post-treatment via flow cytometry. Representative flow cytometry plots (A&C). Frequency of $CD11c^+Cy5^+$ cells (B&D) ($n = 5$). (E) After 30 min of exposure to Cy5-tagged EGFP mRNA nanoparticles, dendritic cells were visualized with confocal microscopy, displaying Cy5-tagged mRNA in red and DAPI in blue. (F) Lysosomes were stained with LysoTracker (green), and the co-localization of Cy5-tagged mRNA with LysoTracker-positive endo/lysosomes was analyzed through confocal microscopy. Nanoparticle-delivered Cy5-tagged EGFP mRNA was shown in red. (G) Pearson's correlation coefficient of DPN reflecting the co-localization of nanoparticles and endo/lysosomes at different time points ($n = 10$). (*$P < 0.001$).**

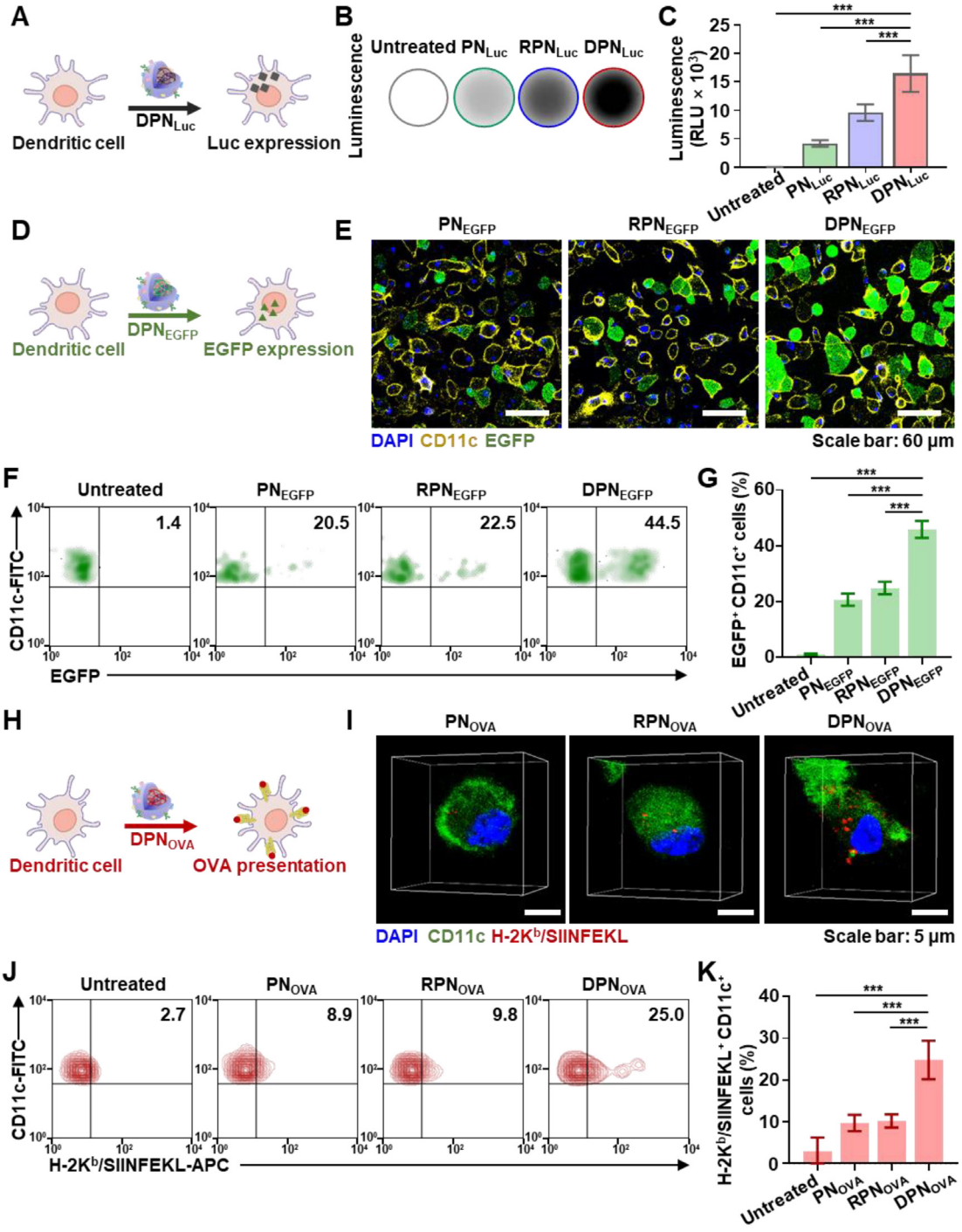

Fig. 4 – Expression of mRNA encoding luciferase, EGFP, or OVA in dendritic cells. (A) Dendritic cells treated with DPN_{Luc}, which encapsulated luciferase mRNA, exhibited luminescence, indicating luciferase expression. (B, C) Luminescence from dendritic cells, either untreated or treated with various nanoparticles, was captured (B) and quantified (C) ($n = 5$). (D) A schematic outlines EGFP mRNA delivery via DPN_{EGFP}, with EGFP expression visualized by confocal microscopy and quantified using flow cytometry. (E) Following treatment with nanoparticles, dendritic cells displayed EGFP expression (green), visualized with confocal microscopy. These cells were also immunostained with PE-conjugated anti-CD11c antibody (yellow) and nuclei were labeled with DAPI (blue). (F, G) Flow cytometry detected EGFP expression in $CD11c^+$ dendritic cells (F) and quantified the $EGFP^+CD11c^+$ cell populations (G) ($n = 5$). (H) An illustration depicts dendritic cells treated with DPN containing OVA mRNA (DPN_{OVA}). (I) Confocal microscopy images showed OVA antigen presentation on the membrane of dendritic cells treated with OVA mRNA delivered via PN_{OVA}, RPN_{OVA}, or DPN_{OVA}, with $CD11c^+$ cells in green and nuclei in blue. (J) Flow cytometry was used to analyze OVA presentation on dendritic cells. (K) Flow cytometry analysis quantified populations of dendritic cells presenting the OVA antigen ($n = 5$). (*$P < 0.001$).**

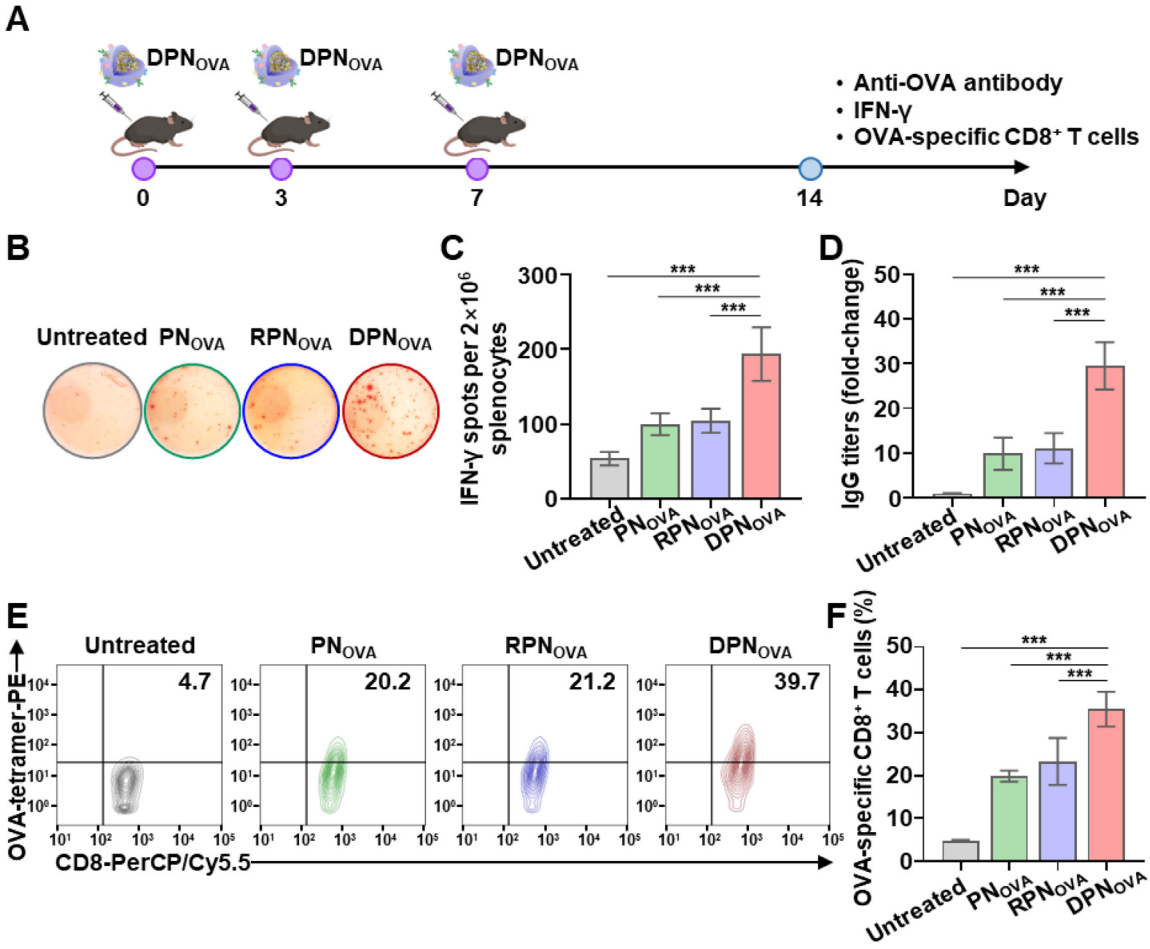

Fig. 5 – *In vivo* immune responses induced by nanoparticles. (A) An illustration outlines the timeline for assessing antigen-specific immune responses induced by nanoparticles. C57BL/6 mice received subcutaneous injections of PN_{OVA}, RPN_{OVA}, or DPN_{OVA} thrice. Blood and spleens were harvested on Day 14 after the first nanoparticle administration for further evaluation. (B) Photographs showed IFN-γ production. Splenocytes underwent stimulation with $OVA_{257–264}$ peptide, followed by an ELISpot assay to quantify IFN-γ production. (C) IFN-γ-positive spot counts were recorded for each group ($n = 5$). (D) Plasma samples were subjected to ELISA to measure anti-OVA IgG antibody levels ($n = 5$). (E, F) After 72 h of $OVA_{257–264}$ peptide stimulation, OVA-specific $CD8^+$ T cell presence was determined using an MHC tetramer for the SIINFEKL OVA epitope. Flow cytometry plots depicted OVA-specific $CD8^+$ T cells following subcutaneous delivery of each formulation (E), with subsequent analysis of OVA-specific $CD8^+$ T cell populations (F) ($n = 5$). (*$P < 0.001$).**

respectively (Fig. 5C). DPN_{OVA} treatment notably increased anti-OVA IgG antibody induction, with antibody levels 3.0 and 2.7 times higher than PN_{OVA} and RPN_{OVA} treatments, respectively (Fig. 5D).

Furthermore, DPN_{OVA} administration led to a significant rise in OVA-specific $CD8^+$ T cell populations. The highest frequency of $CD8^+$ T cells, identified by the MHC tetramer for the OVA epitope SIINFEKL, was observed in the DPN_{OVA}-treated group (Fig. 5E). Compared to PN_{OVA} and RPN_{OVA} groups, the DPN_{OVA}-treated group showed a 1.8-fold and 1.5-fold increase in OVA-specific $CD8^+$ T cell populations (Fig. 5F).

The immune responses induced by DPN_{OVA} underscore the potential of DPN for mRNA vaccine delivery. It was observed that DPN_{OVA} elicited both humoral immune responses and $CD8^+$ T cell responses. The capability to induce both humoral and cellular immune responses widens the application spectrum of DPN for both preventive and therapeutic mRNA vaccines. The induction of OVA-specific cytotoxic T cell response by DPN_{OVA} could be attributed to the delivery of antigen mRNA to dendritic cells, which are key antigen-presenting cells. It has been reported that antigen presentation by dendritic cells can stimulate antigen-specific T cells [26,44,45].

3.5. *Immune responses induced by subcutaneous administration of DPN_{OVA}*

Compared to the untreated group, DPN_{OVA} significantly enhanced DC maturation, as manifested by higher expression of CD40 and CD86 in DC (Fig. S4). The expression levels of CD40 and CD86 exhibited a 2.6-fold and 1.4-fold increase in comparison with the untreated group, respectively (Fig. S4B and S4C). Subcutaneous administrations of DPN_{OVA} stimulated the immune response, as evidenced by enhanced

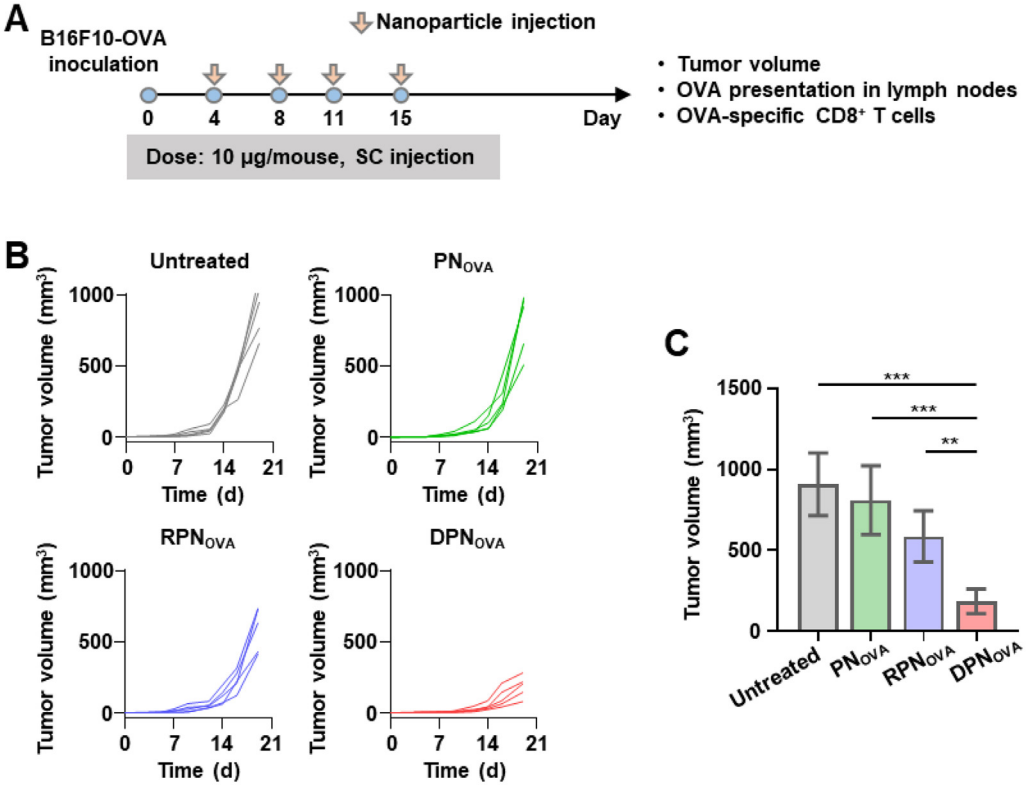

Fig. 6 – Anti-tumor effect of DPN_{OVA}. (A) A schematic illustration depicts the protocol for evaluating DPN's therapeutic efficacy in B16F10-OVA melanoma-bearing C57BL/6 mice. (B) Tumor growth was tracked, presenting individual growth curves for each treatment group ($n = 5$). (C) Comparative analysis of mean tumor volumes across different nanoparticle treatments was conducted ($n = 5$). ($P < 0.01$; ***$P < 0.001$).**

T cell activation (Fig. S4D and S4E). Compared to the untreated group, DPN_{OVA} treatment increased IFN-γ-secreting $CD8^+$ T cells by 2.3-fold and GzmB-secreting $CD8^+$ T cells by 3.3-fold.

3.6. *Anti-tumor effect and antigen-specific immune cell populations*

The efficacy of DPN_{OVA} as a therapeutic antitumor mRNA vaccine was evaluated in B16F10-OVA tumor-bearing mice. Mice were subcutaneously injected four times with various nanoparticles, as depicted in Fig. 6A. The tumor volume was significantly lower in the DPN_{OVA}-treated group compared to groups either untreated or treated with PN_{OVA} or RPN_{OVA} (Fig. 6B). On Day 19 post-tumor inoculation, tumor volumes in the untreated and RPN_{OVA} groups were 4.9 and 3.2 times larger than that in the DPN_{OVA}-treated group, respectively (Fig. 6C). DPN_{OVA} effectively prevented the occurrence of lung metastasis compared to the untreated group, exhibiting a 6-fold decrease in lung tumor nodules (Fig. S5). It is worth noting that therapeutic vaccines are typically administered more frequently than prophylactic cancer vaccines. Therefore, the dosing schedules for prophylactic vaccines require further optimization to maximize their efficacy.

To examine the recruitment of tumor antigen-presenting dendritic cells in the lymph nodes, OVA presentation in $CD11c^+$ cells was analyzed via immunohistochemistry. The DPN_{OVA}-treated group exhibited a notably higher population of OVA-presenting $CD11c^+$ dendritic cells than the control groups (Fig. 7A). Flow cytometry showed that antigen-presenting cells displaying OVA were the most abundant in the DPN_{OVA}-treated group, with 2.0-fold and 1.7-fold increases compared to the untreated and RPN_{OVA}-treated groups, respectively (Fig. 7B and 7C). Moreover, OVA-specific $CD8^+$ cytotoxic T cell populations were significantly elevated in DPN_{OVA}-treated mice, showing 3.8-fold and 1.5-fold higher levels than those in untreated and RPN_{OVA}-treated groups, respectively (Fig. 7D and 7E). In the DPN_{OVA}-treated group, significantly higher populations of anti-tumor cytotoxic T cells were observed compared to the RPN_{OVA}-treated group, exhibiting a 1.6-fold increase in $GzmB^+CD8^+$ T cells (Fig. 7F and 7G) and a 1.5-fold increase in IFN-γ^+CD8^+ T cells (Fig. 7H and 7I). The liver injury and kidney injury parameters, including ALT, AST, ALP, BUN, creatinine, and albumin were in the normal ranges after subcutaneous administration of DPN_{OVA} (Fig. S6B) [46].

Although this study focused on cancer treatment, the dendritic cell-targeted mRNA delivery strategy developed here could extend beyond cancer treatment, for instance, to autoimmune diseases like multiple sclerosis, where dendritic cells play a pivotal role [47]. Given that the induction of tolerogenic dendritic cells or artificial tolerogenic dendritic cells is being actively explored as a treatment for multiple sclerosis [48], our strategy could potentially be exploited to induce immune tolerance by targeting dendritic cells [49].

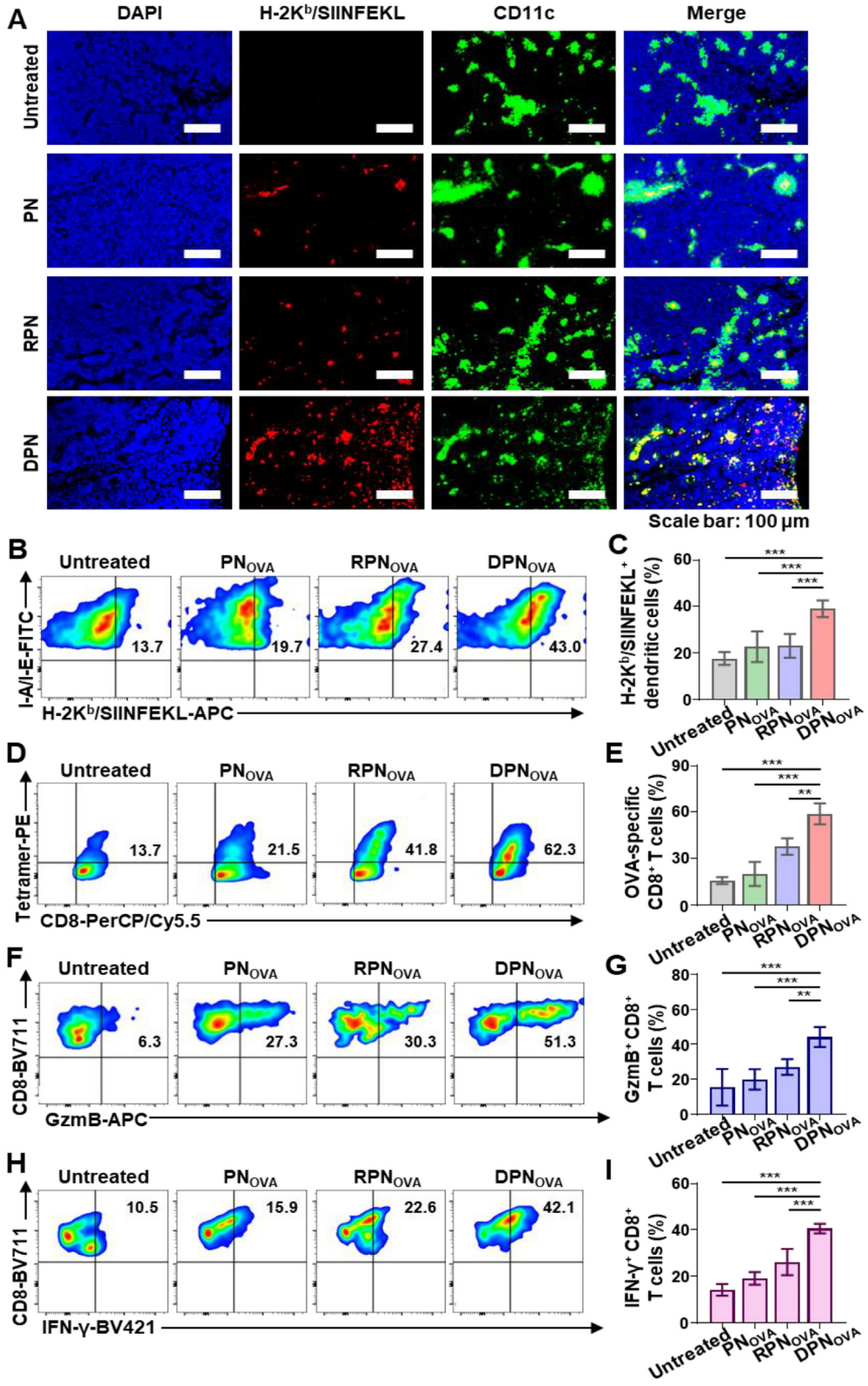

Fig. 7 – OVA-presenting dendritic cells and activation of CD8$^+$ T cells. (A) Immunofluorescence images showed OVA epitope presentation (red) within lymph nodes, with CD11c$^+$ dendritic cells identified using FITC-tagged anti-mouse CD11c antibody (green). (B, C) Flow cytometry provided representative plots (B) and quantified the frequency of OVA-presenting dendritic cells (C) ($n = 5$). (D, E) Representative flow cytometry plots (D) and the frequency of OVA-specific CD8$^+$ T cells (E) were documented ($n = 5$). (F, G) Representative flow cytometry plots (F) and the frequency of GzmB$^+$CD8$^+$ T cells (G) were documented ($n = 5$). (H, I) Representative flow cytometry plots (H) and the frequency of IFN-γ^+CD8$^+$ T cells (I) were determined ($n = 5$). ($P < 0.01$; ***$P < 0.001$).**

Furthermore, the potential of utilizing dendritic cell-derived particles, such as exosomes, for targeted therapy deserves further investigation [50]. It has also been reported that dendritic cell membrane vesicles exhibit a homing effect to the lymph nodes, potentially enhancing robust T cell responses [51]. Therefore, investigating the immunological effects of DPN itself is crucial for developing effective anti-tumor vaccines.

In summary, our study presents a dendritic cell membrane-cloaked nanoparticulate system that enables enhanced mRNA delivery to dendritic cells. The use of dendritic cell membrane coating holds significant implications for cancer immunotherapy and therapies for other diseases involving dendritic cells.

4. Conclusion

Herein, by exploiting the homing effect of the cell membrane, we have constructed a dendritic cell membrane-coated polyplex that exhibited enhanced cellular uptake of mRNA and elevated mRNA expression in antigen-presenting cells. The DPN-mediated improvement in mRNA delivery to antigen-presenting cells induced specific immune responses to mRNA-encoded antigens, showing promising therapeutic effects in the treatment of cancer. This strategy, utilizing the inherent properties of cell membranes, provides new insights into the effective delivery of mRNA and holds significant promise for improving immunotherapy.

Conflicts of interest

The authors report no conflicts of interest. The authors alone are responsible for the content and writing of this article.

Acknowledgments

This research was funded by grants from the National Research Foundation (NRF) of Korea, Ministry of Science and ICT, Republic of Korea (NRF-2021R1A2B5B03002123; NRF-2018R1A5A2024425; NRF-2022M3E5F1017919), and from the Alchemist Project of the Korea Evaluation Institute of Industrial Technology (KEIT 20018560, NTIS 1415184668), the Ministry of Trade, Industry & Energy, Republic of Korea.

Supplementary materials

Supplementary material associated with this article can be found, in the online version, at doi:10.1016/j.ajps.2024.100968.

References

[1] Pollard AJ, Bijker EM. A guide to vaccinology: from basic principles to new developments. Nat Rev Immunol 2021;21(2):83–100.
[2] Gote V, Bolla PK, Kommineni N, Butreddy A, Nukala PK, Palakurthi SS, Khan W. A comprehensive review of mRNA vaccines. Int J Mol Sci 2023;24(3):2700.
[3] Weng Y, Huang Y. Advances of mRNA vaccines for COVID-19: a new prophylactic revolution begins. Asian J Pharm Sci 2021;16(3):263–4.
[4] Kim D, Wu Y, Kim YB, Oh YK. Advances in vaccine delivery systems against viral infectious diseases. Drug Deliv Transl Res 2021;11(4):1401–19.
[5] Byun J, Wu Y, Park J, Kim JS, Li Q, Choi J, et al. RNA nanomedicine: delivery strategies and applications. AAPS J 2023;25(6):95.
[6] Teijaro JR, Farber DL. COVID-19 vaccines: modes of immune activation and future challenges. Nat Rev Immunol 2021;21(4):195–7.
[7] Huang P, Deng H, Zhou Y, Chen X. The roles of polymers in mRNA delivery. Matter 2022;5(6):1670–99.
[8] Suberi A, Grun MK, Mao T, Israelow B, Reschke M, Grundler J, et al. Polymer nanoparticles deliver mRNA to the lung for mucosal vaccination. Sci Transl Med 2023;15(709):eabq0603.
[9] Ben-Akiva E, Karlsson J, Hemmati S, Yu H, Tzeng SY, Pardoll DM, et al. Biodegradable lipophilic polymeric mRNA nanoparticles for ligand-free targeting of splenic dendritic cells for cancer vaccination. Proc Natl Acad Sci USA 2023;120(26):e2301606120.
[10] Yang W, Mixich L, Boonstra E, Cabral H. Polymer-based mRNA delivery strategies for advanced therapies. Adv Healthc Mater 2023;12(15):e2202688.
[11] Fang RH, Gao R, Zhang L. Targeting drugs to tumours using cell membrane-coated nanoparticles. Nat Rev Clin Oncol 2023;20(1):33–48.
[12] Miao Y, Yang Y, Guo L, Chen M, Zhou X, Zhao Y, et al. Cell membrane-camouflaged nanocarriers with biomimetic deformability of erythrocytes for ultralong circulation and enhanced cancer therapy. ACS Nano 2022;16(4):6527–40.
[13] Liu L, Bai X, Martikainen MV, Kårlund A, Roponen M, Xu W, et al. Cell membrane coating integrity affects the internalization mechanism of biomimetic nanoparticles. Nat Commun 2021;12(1):5726.
[14] Parodi A, Quattrocchi N, van de Ven AL, Chiappini C, Evangelopoulos M, Martinez JO, et al. Synthetic nanoparticles functionalized with biomimetic leukocyte membranes possess cell-like functions. Nat Nanotechnol 2013;8(1):61–8.
[15] Lin Y, Yin Q, Tian D, Yang X, Liu S, Sun X, et al. Vaginal epithelial cell membrane-based phototherapeutic decoy confers a “three-in-one” strategy to treat against intravaginal infection of candida albicans. ACS Nano 2023;17(13):12160–75.
[16] Lin Y, Yin Q, Zhuge D, Hu Y, Yang X, Tian D, et al. Enhanced targeting, retention, and penetration of amphotericin B through a biomimetic strategy to treat against vulvovaginal candidiasis. Adv Therap 2022;6:2200086.
[17] Liu S, Xu J, Liu Y, You Y, Xie L, Tong S, et al. Neutrophil-biomimetic “nanobuffer” for remodeling the microenvironment in the infarct core and protecting neurons in the penumbra via neutralization of detrimental factors to treat ischemic stroke. ACS Appl Mater Interfaces 2022;14(24):27743–61.
[18] Tian W, Lu J, Jiao D. Stem cell membrane vesicle–coated nanoparticles for efficient tumor-targeted therapy of orthotopic breast cancer. Polym Adv Technol 2019;30:1051–60.
[19] Liu Y, Rao P, Qian H, Shi Y, Chen S, Lan J, et al. Regulatory fibroblast-like synoviocytes cell membrane coated nanoparticles: a novel targeted therapy for rheumatoid arthritis. Adv Sci 2023;10(4):e2204998.
[20] Tang Q, Sun S, Wang P, Sun L, Wang Y, Zhang L, et al. Genetically engineering cell membrane-coated BTO nanoparticles for MMP2-activated piezocatalysis-immunotherapy. Adv Mater 2023;35(18):e2300964.

[21] Harvey BT, Fu X, Li L, Neupane KR, Anand N, Kolesar JM, et al. Dendritic cell membrane-derived nanovesicles for targeted T cell activation. ACS Omega 2022;7(50):46222–33.
[22] Cao Y, Long J, Sun H, Miao Y, Sang Y, Lu H, et al. Dendritic cell-mimicking nanoparticles promote mRNA delivery to lymphoid organs. Adv Sci 2023;10(33):e2302423.
[23] Hodge AL, Baxter AA, Poon IKH. Gift bags from the sentinel cells of the immune system: the diverse role of dendritic cell-derived extracellular vesicles. J Leukoc Biol 2022;111(4):903–20.
[24] Ghorbaninezhad F, Alemohammad H, Najafzadeh B, Masoumi J, Shadbad MA, Shahpouri M, et al. Dendritic cell-derived exosomes: a new horizon in personalized cancer immunotherapy? Cancer Lett 2023;562:216168.
[25] Liu Q, Rojas-Canales DM, Divito SJ, Shufesky WJ, Stolz DB, Erdos G, et al. Donor dendritic cell-derived exosomes promote allograft-targeting immune response. J Clin Invest 2016;126(8):2805–20.
[26] Le QV, Suh J, Choi JJ, Park GT, Lee J, Shim G, et al. In situ nanoadjuvant-assembled tumor vaccine for preventing long-term recurrence. ACS Nano 2019;13(7):7442–62.
[27] Xu L, Gao F, Fan F, Yang L. Platelet membrane coating coupled with solar irradiation endows a photodynamic nanosystem with both improved antitumor efficacy and undetectable skin damage. Biomaterials 2018;159:59–67.
[28] Zhuang J, Gong H, Zhou J, Zhang Q, Gao W, Fang RH, et al. Targeted gene silencing *in vivo* by platelet membrane-coated metal-organic framework nanoparticles. Sci Adv 2020;6(13):eaaz6108.
[29] Hernández M, Leyva G, Magaña JJ, Guzmán-Vargas A, Felipe C, Lara V, et al. New copolymers as hosts of ribosomal RNA. BMC Chem 2019;13(1):33.
[30] Wang B, Xiong M, Susanto J, Li X, Leung WY, Xu K. Transforming rhodamine dyes for (d) STORM super-resolution microscopy via 1,3-disubstituted imidazolium substitution. Angew Chem Int Ed Engl 2022;61(9):e202113612.
[31] Evans BC, Fletcher RB, Kilchrist KV, Dailing EA, Mukalel AJ, Colazo JM, et al. An anionic, endosome-escaping polymer to potentiate intracellular delivery of cationic peptides, biomacromolecules, and nanoparticles. Nat Commun 2019;10(1):5012.
[32] Chen J, Li J, Zhou J, Lin Z, Cavalieri F, Czuba-Wojnilowicz E, et al. Metal-phenolic coatings as a platform to trigger endosomal escape of nanoparticles. ACS Nano 2019;13(10):11653–64.
[33] Hu B, Li B, Li K, Liu Y, Li C, Zheng L, et al. Thermostable ionizable lipid-like nanoparticle (iLAND) for RNAi treatment of hyperlipidemia. Sci Adv 2022;8(7):eabm1418.
[34] Miao L, Li L, Huang Y, Delcassian D, Chahal J, Han J, et al. Delivery of mRNA vaccines with heterocyclic lipids increases anti-tumor efficacy by STING-mediated immune cell activation. Nat Biotechnol 2019;37(10):1174–85.
[35] Zhang H, You X, Wang X, Cui L, Wang Z, Xu F, et al. Delivery of mRNA vaccine with a lipid-like material potentiates antitumor efficacy through Toll-like receptor 4 signaling. Proc Natl Acad Sci USA 2021;118(6):e2005191118.
[36] Arya S, Lin Q, Zhou N, Gao X, Huang JD. Strong immune responses induced by direct local injections of modified mRNA-lipid nanocomplexes. Mol Ther Nucleic Acids 2020;19:1098–109.
[37] Li F, Zhang XQ, Ho W, Tang M, Li Z, Bu L, et al. mRNA lipid nanoparticle-mediated pyroptosis sensitizes immunologically cold tumors to checkpoint immunotherapy. Nat Commun 2023;14(1):4223.
[38] Sharma R, Lee JS, Bettencourt RC, Xiao C, Konieczny SF, Won YY. Effects of the incorporation of a hydrophobic middle block into a PEG-polycation diblock copolymer on the physicochemical and cell interaction properties of the polymer-DNA complexes. Biomacromolecules 2008;9(11):3294–307.
[39] Liu WL, Zou MZ, Liu T, Zeng JY, Li X, Yu WY, et al. Expandable immunotherapeutic nanoplatforms engineered from cytomembranes of hybrid cells derived from cancer and dendritic cells. Adv Mater 2019;31(18):e1900499.
[40] Fang RH, Kroll AV, Gao W, Zhang L. Cell membrane coating nanotechnology. Adv Mater 2018;30(23):e1706759.
[41] Ma X, Kuang L, Yin Y, Tang L, Zhang Y, Fan Q, et al. Tumor-antigen activated dendritic cell membrane-coated biomimetic nanoparticles with orchestrating immune responses promote therapeutic efficacy against glioma. ACS Nano 2023;17(3):2341–55.
[42] Mahajan S, Tang T. Polyethylenimine-DNA nanoparticles under endosomal acidification and implication to gene delivery. Langmuir 2022;38(27):8382–97.
[43] Rui Y, Wilson DR, Tzeng SY, Yamagata HM, Sudhakar D, Conge M, et al. High-throughput and high-content bioassay enables tuning of polyester nanoparticles for cellular uptake, endosomal escape, and systemic *in vivo* delivery of mRNA. Sci Adv 2022;8(1):eabk2855.
[44] Jneid B, Bochnakian A, Hoffmann C, Delisle F, Djacoto E, Sirven P, et al. Selective STING stimulation in dendritic cells primes antitumor T cell responses. Sci Immunol 2023;8(79):eabn6612.
[45] Yang C, Zhang F, Chen F, Chang Z, Zhao Y, Shao D, et al. Biomimetic nanovaccines potentiating dendritic cell internalization via CXCR4-mediated macropinocytosis. Adv Healthc Mater 2023;12(5):e2202064.
[46] Loeb WF, Quimby FW. The clinical chemistry of laboratory animals. 2nd ed. Philadelphia: Taylor & Francis USA; 1999.
[47] Bourque J, Hawiger D. Life and death of tolerogenic dendritic cells. Trends Immunol 2023;44(2):110–18.
[48] Park J, Le QV, Wu Y, Lee J, Oh YK. Tolerogenic nanovaccine for prevention and treatment of autoimmune encephalomyelitis. Adv Mater 2023;35(1):e2202670.
[49] Cifuentes-Rius A, Desai A, Yuen D, Johnston APR, Voelcker NH. Inducing immune tolerance with dendritic cell-targeting nanomedicines. Nat Nanotechnol 2021;16(1):37–46.
[50] Dong H, Li Q, Zhang Y, Ding M, Teng Z, Mou Y. Biomaterials facilitating dendritic cell-mediated cancer immunotherapy. Adv Sci 2023;10(18):e2301339.
[51] Xu J, Liu H, Wang T, Wen Z, Chen H, Yang Z, et al. CCR7 mediated mimetic dendritic cell vaccine homing in lymph node for head and neck squamous cell carcinoma therapy. Adv Sci 2023;10(17):e2207017.